Inorganic Chemistry Cite This: Inorg. Chem. 2019, 58, 15971–15982

pubs.acs.org/IC

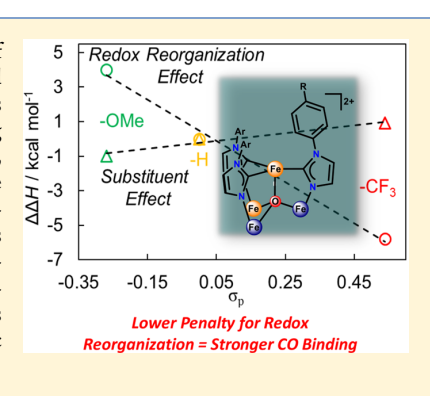
Remote Ligand Modifications Tune Electronic Distribution and Reactivity in Site-Differentiated, High-Spin Iron Clusters: Flipping Scaling Relationships

Charles H. Arnett, Jens T. Kaiser, and Theodor Agapie*

Division of Chemistry and Chemical Engineering, California Institute of Technology, Pasadena, California 91125, United States

Supporting Information

ABSTRACT: We report the synthesis, characterization, and reactivity of [LFe₃O(RArIm)₃Fe][OTf]₂, the first Hammett series of a site-differentiated cluster. The cluster reduction potentials and CO stretching frequencies shift as expected on the basis of the electronic properties of the ligand: electron-donating substituents result in more reducing clusters and weaker C-O bonds. However, unusual trends in the energetics of their two sequential CO binding events with the substituent σ_p parameters are observed. Specifically, introduction of electrondonating substituents suppresses the first CO binding event ($\Delta\Delta H$ by as much as 7.9 kcal mol⁻¹) but enhances the second ($\Delta\Delta H$ by as much as 1.9 kcal mol⁻¹). Xray crystallography, including multiple-wavelength anomalous diffraction, Mössbauer spectroscopy, and SQUID magnetometry, reveal that these substituent effects result from changes in the energetic penalty associated with electronic redistribution within the cluster, which occurs during the CO binding event.



INTRODUCTION

The reactivity of transition-metal ions is sensitive to their local environment, 1,2 enabling the rational development and optimization of catalysts on the basis of established structure-function relationships. However, because many of the thermodynamic properties central to their reactivity are highly correlated, 3-5 ligand modifications which enhance one measure of reactivity (e.g. reduction potential) may adversely affect another (e.g. acidity, hydricity, ligand binding affinity).6-8 Breaking, or inverting, these traditional scaling relationships can prove advantageous in fine-tuning the reactivity and/or selectivity of transition-metal-based catalysts. 9-13 For example, incorporation of trimethylanilinium groups into the backbone of a tetraphenylporphyrin results in electrocatalysts for CO₂ reduction which operate with higher efficiency at lower overpotential due to stabilization of the initial Fe⁰-CO₂ adduct, breaking the correlation between activity and overpotential.

In comparison to monometallic systems, the influence of changes in the first and second coordination sphere on the properties of metal clusters is poorly understood, 14-16 despite the fact that catalysts which incorporate multiple metal centers are common in biological systems and mediate challenging multielectron transformations. 17-22 Although only a subset of the metal ions within the cluster are believed to be involved in substrate binding and functionalization, the remote metals may significantly affect the properties and activity of the reactive site.^{23–28} For example, varying the identity of the pendant group 13 metal in a series of heterobimetallic [MNi] (M = Al, Ga, In) complexes tunes their H_2 and N_2 binding affinities²³ as well as their activity toward olefin hydrogenation.²⁹ A

heterobimetallic Zr/Co complex activates O_2^{25} and organic azides²⁶ at a Zr^{IV} center, with electrons delivered to the substrate by the remote redox-active cobalt center. Conversely, proximal redox-inactive metals have been shown to induce inverse linear free energy relationships in the rates of C-H oxidation⁹ and Mn^VN coupling.¹⁰ Studies from our laboratory demonstrate that remote metal sites influence small-molecule activation, 30-32 bond dissociation free energies, 33,34 and oxygen atom transfer³⁵ without formally changing the oxidation state of the metal site directly involved in substrate binding. The close proximity of multiple redox-active metal centers in a site-differentiated cluster may afford unique opportunities to challenge traditional scaling relationships, though such an approach has not been realized because of the synthetic challenges associated with controlling cluster nuclearity and geometry in common self-assembly reactions.³

To facilitate (electronic) structure–function studies, 37-41 our group and others have employed polynucleating ligand scaffolds to template the organization of multiple metal centers. 42-47 Herein, we report the synthesis and characterization of a unique Hammett series of a site-differentiated cluster, [LFe₃O(RArIm)₃Fe][OTf]₂ (Figure 1), which reversibly binds up to two molecules of CO. The redox properties of the cluster are dependent on the electronic nature of the substituent ($\Delta E_{1/2} = 270-310$ mV), with electron-releasing substituents resulting in cathodic shifts. Unexpectedly, introduction of electron-donating substituents suppresses the first CO binding event of the cluster ($\Delta \Delta H$ by as much as 7.9

Received: August 14, 2019 Published: November 18, 2019



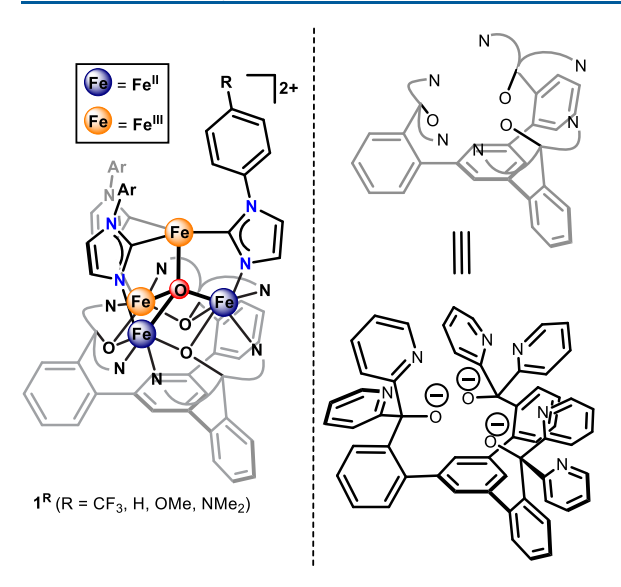


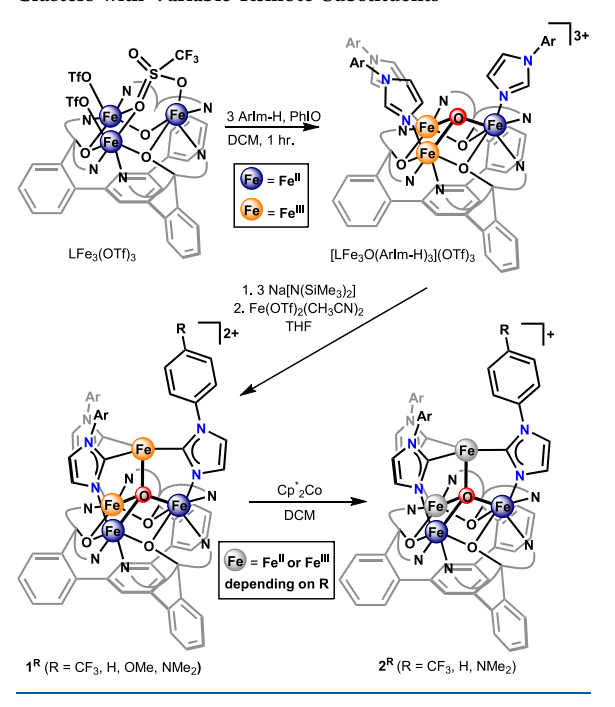
Figure 1. General molecular structure of $[LFe_3O(^RArIm)_3Fe][OTf]_2$, supported by imidazolates and a 1,3,5-triarylbenzene-based ligand. The inset shows the coloring scheme for the metal oxidation states.

kcal mol^{-1}). Even more surprising, the opposite trend is observed for the second CO binding event, which is *enhanced* by electron-donating substituents ($\Delta\Delta H$ by as much as 1.9 kcal mol^{-1}). Crystallographic, spectroscopic, and magnetic studies enabled us to deconvolute the effect of ligand modification at specific sites within the cluster. These studies suggest that electron-releasing substituents enlarge the energetic penalty associated with electronic redistribution within the cluster, an essential feature of the first CO binding event. Binding of the second molecule of CO does not require an internal electron transfer, which explains why the second binding constant increases as the clusters become more electron rich.

■ RESULTS AND DISCUSSION

Synthesis and Electrochemistry. The complexes $[LFe_3O(^{pCF3}ArIm)_3Fe][OTf]_2$ (1^{CF3}) , $[LFe_3O(^{pOMe}ArIm)_3Fe][OTf]_2$ (1^{OMe}) , and $[LFe_3O(^{pNMe2}ArIm)_3Fe][OTf]_2$ (1^{NMe2}) were synthesized in a manner similar to that recently described for $[LFe_3O(PhIm)_3Fe][OTf]_2$ (1^H) (Scheme 1). OAlthough high-quality crystal structures could not be obtained for 1^{OMe} or 1^{NMe2} , their H NMR spectra are strikingly similar to those of the structurally characterized clusters 1^{CF3} and 1^H (Figure 21 in the Supporting Information). Moreover, the ESI mass spectra of 1^{OMe} and 1^{NMe2} feature peaks at m/z 809 and 827, respectively, consistent with $[LFe_3O(^{pOMe}ArIm)_3Fe]^{2+}$ and $[LFe_3O(^{pNMe2}ArIm)_3Fe]^{2+}$ formulations.

Scheme 1. Modular Synthesis of Site-Differentiated Iron Clusters with Variable Remote Substituents



illustrated by the linear correlation of the measured $E_{1/2}$ values with their Hammett $\sigma_{\rm p}$ parameters (Figure 2B). The half-wave potentials of the Fe^{II}₃Fe^{III}/Fe^{II}₂Fe^{III}₂ redox event are shifted over a 310 mV range from -0.87 V for $1^{\rm CF3}$ to -1.18 V for $1^{\rm NMe2}$, suggesting a significant effect of remote ligand substitution on the energy of the redox-active orbital(s) associated with the [Fe₃(μ_4 -O)Fe]core. Likewise, the half-wave potentials of the Fe^{II}₂Fe^{III}₂/Fe^{II}Fe^{III}₃ redox event are tuned over a similar range (270 mV) from +0.02 V for $1^{\rm CF3}$ to -0.25 V for $1^{\rm NMe2}$.

Spectroscopic Studies of [LFe₃O(RArlm)₃Fe]²⁺ Clus**ters.** Although the electrochemical properties of $\mathbf{1}^{R}$ (R = CF₃, H, OMe, NMe₂) trend with the substituent σ_p parameters, spectroscopic studies reveal only subtle differences in their electronic ground state. 49 The zero-field 57Fe Mössbauer spectra of 1 CF3 (Figure 74 in the Supporting Information) and 1^{NMe2} (Figure 75 in the Supporting Information) are qualitatively similar to that of 1^H ³⁰ Spectral simulations reveal the presence of two iron subsites (50% total iron) with Mössbauer parameters ($\delta \approx 1$ mm/s, $|\Delta E_Q| \approx 3$ mm/s) diagnostic of high-spin, six-coordinate Fe^{II} centers, $^{30-32,34,35,51}$ indicating a [Fe^{II}₂Fe^{III}] assignment of the redox state of the triiron core. Moreover, the isomer shifts associated with the apical iron centers of 1^{CF3} , 1^{H} , and 1^{NMe2} ($\delta = 0.19 - 0.22 \text{ mm/s}$) are consistent with an Fe^{III} formulation. ⁵² The EPR spectra of 1^{CF3} and 1^{NMe2} (Figure 71 in the Supporting Information), collected in parallel mode at 4.5 K in a propionitrile/ butyronitrile (4/5) glass, all exhibit a feature at $g \approx 17.2$ assigned to a transition within the $M_s = \pm 4$ doublet of an S = 4spin system (D < 0). This assignment is consistent with variable-temperature magnetic susceptibility measurements on 1^{CF3} (Figure 50 in the Supporting Information) and 1^{NMe2} (Figure 53 in the Supporting Information), which plateau ($\mathbf{1}^{\text{CF3}}$, ~8.8 cm³ K mol⁻¹; $\mathbf{1}^{\text{NMe2}}$, ~9.3 cm³ K mol⁻¹) near the

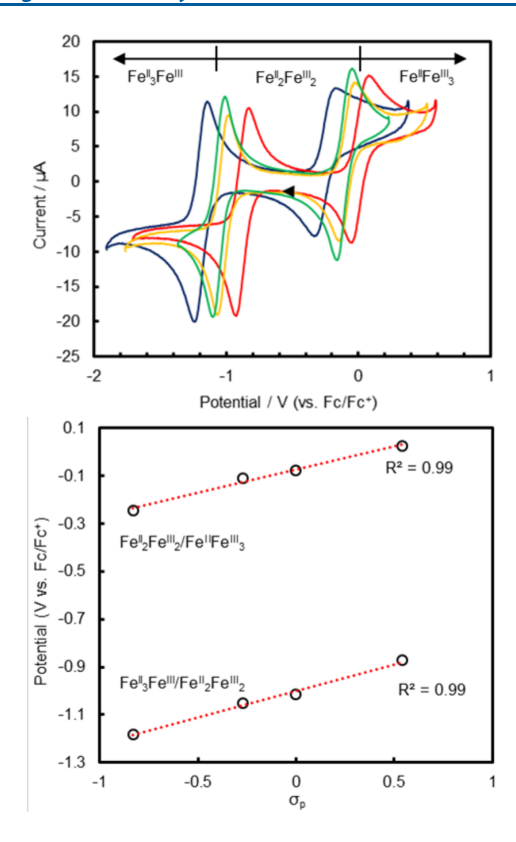


Figure 2. (A) Cyclic voltammograms of $\mathbf{1}^{\text{CF3}}$ (red), $\mathbf{1}^{\text{H}}$ (orange), $\mathbf{1}^{\text{OMe}}$ (green), and $\mathbf{1}^{\text{NMe2}}$ (blue) in CH₂Cl₂ (0.1 M $[n\text{Pr}_4\text{N}][\text{BAr}^{\text{F}}_{24}]$ supporting electrolyte). Scan rate: 100 mV/s. (B) Plot of $E_{1/2}(\text{Fe}^{\text{II}}_2\text{Fe}^{\text{III}}_2/\text{Fe}^{\text{III}}_3)$ (top) and $E_{1/2}(\text{Fe}^{\text{II}}_3\text{Fe}^{\text{III}}/\text{Fe}^{\text{II}}_2\text{Fe}^{\text{III}}_2)$ (bottom) vs Hammett substituent constants (σ_{p}) for $\mathbf{1}^{\text{R}}$ (R = CF₃, H, OMe, NMe₂), respectively.

expected spin-only value for an isolated S = 4 center (10 cm³ K mol⁻¹).

Synthesis and X-ray Diffraction Studies of [LFe₃O-(RArlm)₃Fe]⁺ Clusters. Consistent with their electrochemical behavior, 1^{CF3}, 1^H, and 1^{NMe2} can be reduced with 1 equiv of Cp*₂Co, affording complexes with nearly identical ¹H NMR features (Figure 22 in the Supporting Information). Structural characterization confirmed the identity of these paramagnetic compounds as [LFe₃O(PGF3ArIm)₃Fe][OTf] (2^{CF3}, Figure 3A), [LFe₃O(PhIm)₃Fe][BF₄] (2^H, prepared by reduction of 2^H to the all-ferrous cluster followed by reoxidation with [Cp₂Co][BF₄], Figure 3B), and [LFe₃O(PNMe2ArIm)₃Fe][BF₄] (2^{NMe2}, Figure 3C), respectively. Upon reduction, the Fe4–O1 distance of 1^{CF3} (ca. 1.80 Å) elongates to 1.897(1) Å (Table 1), suggesting a ferrous oxidation state assignment for the

Table 1. Summary of Selected Bond Lengths (Å)

| Bond | $1^{\mathrm{H}a}$ | 2 ^{CF3} | 2^{H} | 2^{NMe2} |
|----------------------------|-------------------|------------------|----------|-------------------|
| Fe1-O1 | 2.148(2) | 2.068(2) | 2.091(1) | 2.063(2) |
| Fe2-O1 | 1.983(2) | 1.933(2) | 1.881(1) | 1.986(2) |
| Fe3-O1 | 2.093(2) | 2.074(2) | 2.108(1) | 2.097(2) |
| Fe4-O1 | 1.813(2) | 1.897(1) | 1.881(1) | 1.839(2) |
| Fe1-N11 | 2.144(3) | 2.145(2) | 2.164(2) | 2.164(2) |
| Fe2-N9 | 2.131(2) | 2.133(2) | 2.121(2) | 2.156(2) |
| Fe3-N7 | 2.137(3) | 2.169(2) | 2.174(2) | 2.178(2) |
| Fe4-C60 | 2.068(3) | 2.087(2) | 2.093(2) | 2.071(2) |
| Fe4-C69 | 2.063(3) | 2.107(2) | 2.102(2) | 2.075(3) |
| Fe4-C78 | 2.063(3) | 2.084(2) | 2.082(2) | 2.082(3) |
| ^a Data taken fi | om ref 30. | | | |

apical iron in 2^{CF3} . Moreover, the long Fe1–O1 (2.068(2) Å) and Fe3–O1 (2.074(2) Å) distances and short Fe2–O1 (1.933(2) Å) bond length of 2^{CF3} are consistent with maintaining the $[\text{Fe}^{\text{II}}_{2}\text{Fe}^{\text{III}}]$ redox level of the basal triiron core observed in 1^{CF3} . Similar Fe–O1 bond lengths are observed for 2^{H} (Table 1), indicating that the incorporation of

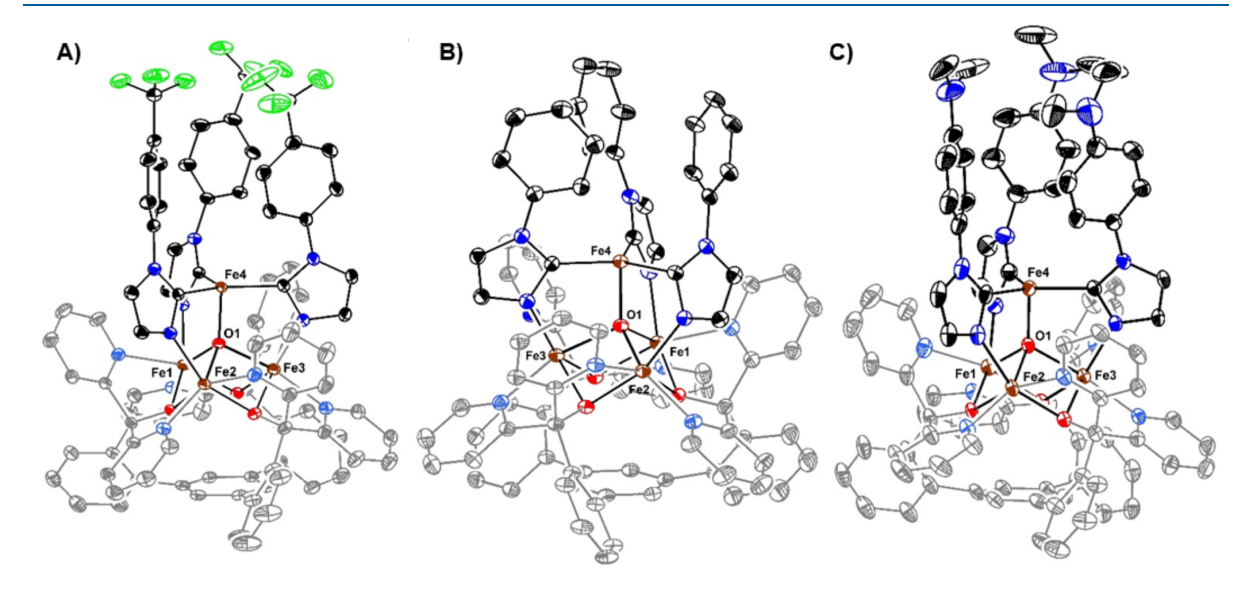


Figure 3. Solid-state structures of 2^{CF3} , 2^H , and 2^{NMe2} : (A) $[LFe_3O(^{pCF3}ArIm)_3Fe][OTf]$ (2^{CF3}); (B) $[LFe_3O(PhIm)_3Fe][BF_4](2^H)$; (C) $[LFe_3O(^{pNMe2}ArIm)_3Fe][BF_4]$ (2^{NMe2}). Hydrogen atoms and outer-sphere counterions are not shown for clarity.

electron-withdrawing trifluoromethyl substituents does not significantly perturb the ground-state electron distribution within the $[LFe_3O(^RArIm)_3Fe]^+$ core.

Remarkably, however, the solid state structure of 2NMe2 reveals a significant influence of remote ligand modification on the redox distribution of the $[LFe_3O(^RArIm)_3Fe]^+$ cluster. The Fe4–O1 bond length of 2^{NMe2} (1.839(2) Å, Table 1) is substantially shorter than those of 2^{CF3} (1.897(1) Å) or 2^H (1.881(1) Å), suggesting that the incorporation of electrondonating dimethylamino substituents favors the localization of ferric character at the apical iron center. This shift in the electron distribution is supported by an elongation in the Fe2-O1 distance from 1.933(2) Å in 2^{CF3} or 1.881(1) Å in 2^{H} to 1.986(2) Å in 2^{NMe2} (Table 1), indicating a more reduced [Fe^{II}₃] triiron core in 2^{NMe2} . Consistent with this assignment, an elongation of the [Fe1|Fe2|Fe3] centroid-O1 distance is observed from 0.957(2) Å in 2^{H} to 1.015(2) Å in 2^{NMe2} . Admittedly, the Fe2–O1 distance of 2^{NMe2} remains somewhat short in comparison to other core Fe^{II}-O1 distances (average ~2.07 Å),30,32 though this may simply be a manifestation of the rigidity of the supporting ligand. Despite differences in the Fe–O1 bond lengths of 2^{CF3} and 2^{NMe2} , the volume of the tetrametallic core remains nearly constant (average Fe-Fe separations: 3.36(4) vs 3.37(3) Å). The constrained volume of the $[Fe_3(\mu_4-O)Fe]$ core may prevent a more dramatic elongation of the Fe2–O1 distance of 2^{NMe2} in response to charge redistribution induced by remote modification of the ligand. The higher sensitivity of the apical iron to the electronic nature of the remote substituents likely results from the fact that, while these substituted imidazolates bridge Fe4 to the basal triiron core, only Fe4 is bound to all three.

⁵⁷Fe Mössbauer Spectroscopy of [LFe₃O(^RArlm)₃Fe]⁺ Clusters. In order to obtain additional insight into the effect of remote ligand modifications on electron distribution, 2^{CF3} and 2^{NMe2} were studied by ⁵⁷Fe Mössbauer spectroscopy. The Mössbauer spectrum of 2^{CF3} (80 K, Figure 4 top) features only three well-resolved resonances, albeit with discernible shoulders near the Lorentzian features around -0.5 and 3 mm/s, respectively. A satisfactory simulation of the experimental spectrum requires at least three distinct iron subsites which, on the basis of the relative intensity of the resonance near 3 mm/s, occur in a 2:1:1 ratio. Two reasonable simulations were obtained (Figures 76 and 77 in the Supporting Information), both of which afford Mössbauer parameters for one subsite (50% total iron) which are consistent with the presence of two high-spin, six-coordinate Fe^{II} centers ($\delta \approx 1.1$ mm/s, $|\Delta E_Q| \approx 3.2$ mm/s) within the triiron core. $^{30-32,34,35,51}$ The relative intensity of the sharp resonance near 1 mm/s indicates the presence of one ferric ion whose isomer shift and quadrupole splitting depend on how the Lorentzian feature near -0.5 mm/s is modeled, with δ bounded between 0.34 and 0.47 mm/s. Isomer shifts in this range are common for high-spin, six-coordinate ferric centers in O/N-rich ligand environments, 59-63 suggesting a [Fe^{II}₂Fe^{III}] redox level for the triiron core identical with that inferred from the solid-state structure. The shoulder observed to the left of the Lorentzian feature around 3 mm/s is attributed to a third ferrous site with a lower isomer shift ($\delta \approx 0.8 \text{ mm/s}$) and lower quadrupole splitting ($|\Delta E_{\rm Q}| \approx 2.7$ mm/s). A similar shoulder is observed in the Mössbauer spectra of 2H 30 and [LFe₃O(PhPz)₃Fe][OTf].³² This shoulder, which is absent in the spectrum of the one-electron-oxidized cluster 1^{CF3} (Figure 74 in the Supporting Information) has been assigned to a

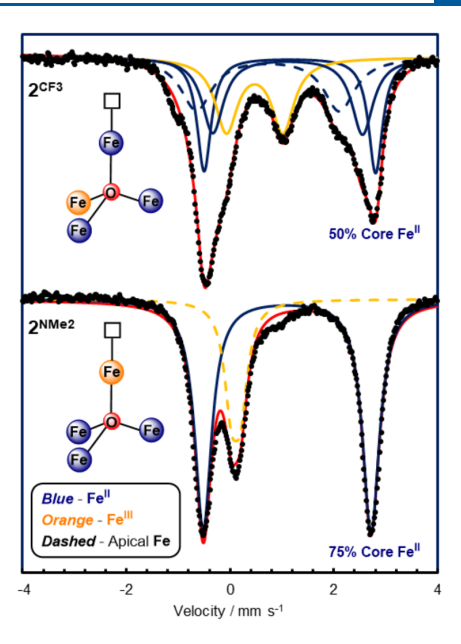


Figure 4. Remote ligand modifications tune redox distribution in a series of site-differentiated $[LFe_3O(^RArIm)_3Fe]^+$ clusters: (top) zero field ^{57}Fe Mössbauer spectrum (80 K, microcrystalline material) of $[LFe_3O(^{PCF3}ArIm)_3Fe][OTf]$ ($\mathbf{2}^{CF3}$); (bottom): zero field ^{57}Fe Mössbauer spectrum (80 K, microcrystalline material) of $[LFe_3O(^{PNMe2}ArIm)_3Fe][OTf]$ ($\mathbf{2}^{NMe2}$). For additional simulation details, see the Supporting Information.

resonance of the apical Fe^{II} center. 30,32 Due to its lower coordination number and softer (C rich) ligand environment, a smaller isomer shift is anticipated for the apical ferrous site in comparison to the pseudo-octahedral Fe^{II} centers of the triiron core. 64 The final model (Table 2) affords an isomer shift of 0.73 mm/s (| $\Delta E_{\rm O}| \approx 2.76$ mm/s) for the trigonal-pyramidal ferrous site of $2^{\rm CF3}$, a value similar to those reported for four-coordinate, high-spin Fe^{II} centers supported by multidentate N-heterocyclic carbene ligand scaffolds. 65,66

On the other hand, the Mössbauer spectrum of 2NMe2 (Figure 4, bottom) is distinct from those of 2^{CF3} and 2^H, indicating a change in the electronic structure. Most notably, the sharp resonance near 1 mm/s observed in the spectra of 2^{CF3}, 2^H, and [LFe₃O(PhPz)₃Fe][OTf]³² is absent. Instead, a sharp, nearly isotropic signal is observed at 0.11 mm/s, indicating a significantly lower isomer shift for the ferric subsite of 2NMe2. Six-coordinate, high-spin FeIII complexes are not known to exhibit isomer shifts lower than ~0.35 mm/s. As such, the quadrupole doublet for the ferric subsite does not originate from within the triiron core. Isomer shifts of ~0.20 mm/s are commonly observed for four-coordinate, high-spin ferric iron complexes in soft ligand environments, suggesting an Fe^{III} assignment for the apical metal center.⁵² Consistent with this assignment, the isomer shift of the apical iron center in 2^{NMe2} ($\delta = 0.11$ mm/s) does not differ significantly from that in 1^{NMe2} ($\delta = 0.22$ mm/s, see Figure 75 in the Supporting Information). For comparison, a substantially larger difference is observed in the isomer shifts associated with the apical iron center in 2^{CF3} ($\delta = 0.73 \text{ mm/s}$) in comparison to 1^{CF3} ($\delta =$ 0.19 mm/s). Furthermore, the presence of three sixcoordinate, high-spin ferrous centers in the triiron core of 2NMe2 is supported by the Mössbauer parameters of the

Table 2. Summary of Mössbauer Parameters

| compd no. | complex | $\delta \; (\text{mm/s})$ | $ \Delta E_{\rm Q} \ ({\rm mm/s})$ | amount (%) |
|-------------------|-------------------------------------|---------------------------|-------------------------------------|------------|
| 1 ^{CF3} | $[LFe_3O(^{pCF3}ArIm)_3Fe][OTf]_2$ | 1.10 | 3.17 | 25 |
| | | 1.16 | 2.80 | 25 |
| | | 0.39 | 0.39 | 25 |
| | | 0.19 | 1.24 | 25 |
| 1 ^{NMe2} | $[LFe_3O(^{pNMe2}ArIm)_3Fe][OTf]_2$ | 1.02 | 2.89 | 25 |
| | | 1.09 | 3.30 | 25 |
| | | 0.39 | 0.45 | 25 |
| | | 0.22 | 1.10 | 25 |
| 2 ^{CF3} | $[LFe_3O(^{pCF3}ArIm)_3Fe][OTf]$ | 1.11 | 2.88 | 25 |
| | | 1.15 | 3.31 | 25 |
| | | 0.47 | 1.09 | 25 |
| | | 0.73 | 2.76 | 25 |
| 2 ^{NMe2} | $[LFe_3O(^{pNMe2}ArIm)_3Fe][OTf]$ | 1.10 | 3.23 | 75 |
| | | 0.11 | 0.18 | 25 |

remaining subsite (δ = 1.10 mm/s, $|\Delta E_Q|$ = 3.23 mm/s, 75% total iron, Table 2).

Multiple-Wavelength Anomalous Diffraction. Further insight into the electronic structure of 2^{CF3} was sought by multiple-wavelength anomalous X-ray diffraction (MAD). Inelastic scattering of X-rays results in a wavelength dependence of the atomic scattering factors: $f_i(\lambda) = f_i^0 + f_i'(\lambda) + f_i'(\lambda)$ $if_i^{\prime\prime}(\lambda)$, where $f_i^{\prime}(\lambda)$ and $f_i^{\prime\prime}(\lambda)$ are the real and imaginary components of the anomalous scattering due to the absorption of X-rays by element i. 67,68 Thus, MAD experiments can provide information on the metal oxidation state and coordination geometry, similarly to XANES, but in a sitespecific manner for individual metal sites within a cluster. 15,69 Unfortunately, however, only $f_i^{\prime\prime}(\lambda)$ is directly proportional to absorption and, for centrosymmetric crystals such as the clusters discussed herein, $f_i^{\prime\prime}(\lambda)$ cannot be refined directly. In principle, analysis of the $f_i'(\lambda)$ spectra could provide similar site-specific information; however, their interpretation is not straightforward and studies of well-defined model clusters are limited. $^{70-73}$ A plot of the refined $f_i'(\lambda)$ values for Fe1–Fe4 as a function of energy for 2^{CF3} (Figure 5) clearly distinguishes the unique coordination environment of Fe4 from Fe1-Fe3. The $f'(\lambda)$ curves of the six-coordinate, high-spin ferrous sites Fe1 and Fe3 are broader and have lower energy minima in

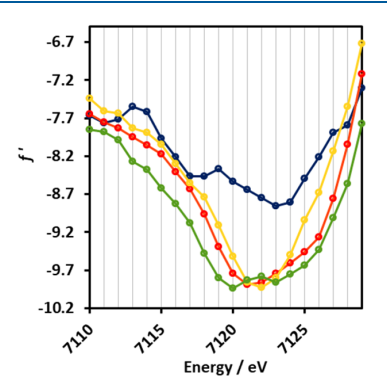


Figure 5. Plot of refined f' values for Fe1 (green), Fe2 (yellow), Fe3 (red), and Fe4 (blue) as a function of energy for $\mathbf{2^{CF3}}$. Atom labels are the same as those used in the structure of $\mathbf{2^{CF3}}$ in Figure 3A. Selected bond lengths are included in Table 1. For additional refinement details, see the Supporting Information.

comparison to those of the six-coordinate ferric site Fe2. Although the effects of radiation damage are apparent in the higher energy data sets (Figure 89 in the Supporting Information), the MAD data for 2^{CF3} correlate well with the oxidation state distribution inferred by traditional X-ray crystallography and ⁵⁷Fe Mössbauer spectroscopy, which indicate an Fe(II) formulation for both Fe1 and Fe3.

SQUID Magnetometry for [LFe₃O-(RArlm)₃Fe]+Clusters. To elucidate the effect of redox distribution on the exchange coupling, variable-temperature magnetic susceptibility measurements were performed on 2^{CF3} $2^{\rm H}$, and $2^{\rm NMe2}$ in the temperature range 1.8–300 K at 0.1 T (Figure 6). The value of $\chi_{\rm M}T$ for $2^{\rm NMe2}$ at 300 K (6.35 cm³ K mol⁻¹) deviates significantly from the spin-only value (13.38 cm³ K mol⁻¹) anticipated for uncoupled Fe^{II} (S = 2) and Fe^{III} (S = 5/2) centers, indicating the presence of antiferromagnetic coupling. However, $\chi_{\rm M}T$ increases gradually as the temperature is lowered (Figure 6, blue trace), eventually reaching a plateau (7.87 cm³ K mol⁻¹) between 10 and 40 K corresponding to the expected spin-only value for an isolated S = 7/2 center (g =2.00). The near-ideal Curie behavior observed between 10 and 40 K suggests that excited states with $S \neq 7/2$ are not thermally accessible. An exchange coupling model ($J_{14} = J_{34}$; J_{12} = I_{23} , numerical subscripts chosen to be consistent with atom labels in the crystal structures) based on the pseudo-C_s symmetry of the $[Fe_3(\mu_4-O)Fe]$ core was employed to simulate the experimental data according to the spin Hamiltonian H = $-2\sum I_{ij}(S_i \cdot S_j)$. The effective exchange coupling constants obtained from these simulations $(J_{14} = J_{34} = -29 \text{ cm}^{-1}, J_{24} = -40 \text{ cm}^{-1}, J_{12} = J_{23} = -3.4 \text{ cm}^{-1}, J_{13} = -0.8 \text{ cm}^{-1})$ reveal that the S = 7/2 ground state originates from spin frustration of the triiron core due to strong antiferromagnetic interactions of Fe1/Fe2/Fe3 with the apical Fe^{III} center. The larger value of J_{24} (in comparison to $J_{14} = J_{34}$) is consistent with the shorter Fe2-O1 distance observed in the solid-state structure. Consistent with the S = 7/2 ground state inferred from magnetic susceptibility measurements, magnetization saturation for 2^{NMe2} occurs at 6.6 μ_{B} at 1.8 K and 7 T, near the expected M = gS limit for g = 2.00. Simulations according to the system spin Hamiltonian $H = DS_z^2 + E(S_x^2 + S_y^2) + g\mu_B S \cdot H$ best reproduce the experimental data assuming S = 7/2 with g = 1.92, D = -0.21 cm⁻¹, and |E/D| = 0 (Figure 69 in the Supporting Information).

In contrast to the gradual rise in $\chi_{\rm M}T$ observed for $2^{\rm NMe2}$, the molar susceptibilities of $2^{\rm CF3}$ (Figure 6, red trace) and $2^{\rm H}$

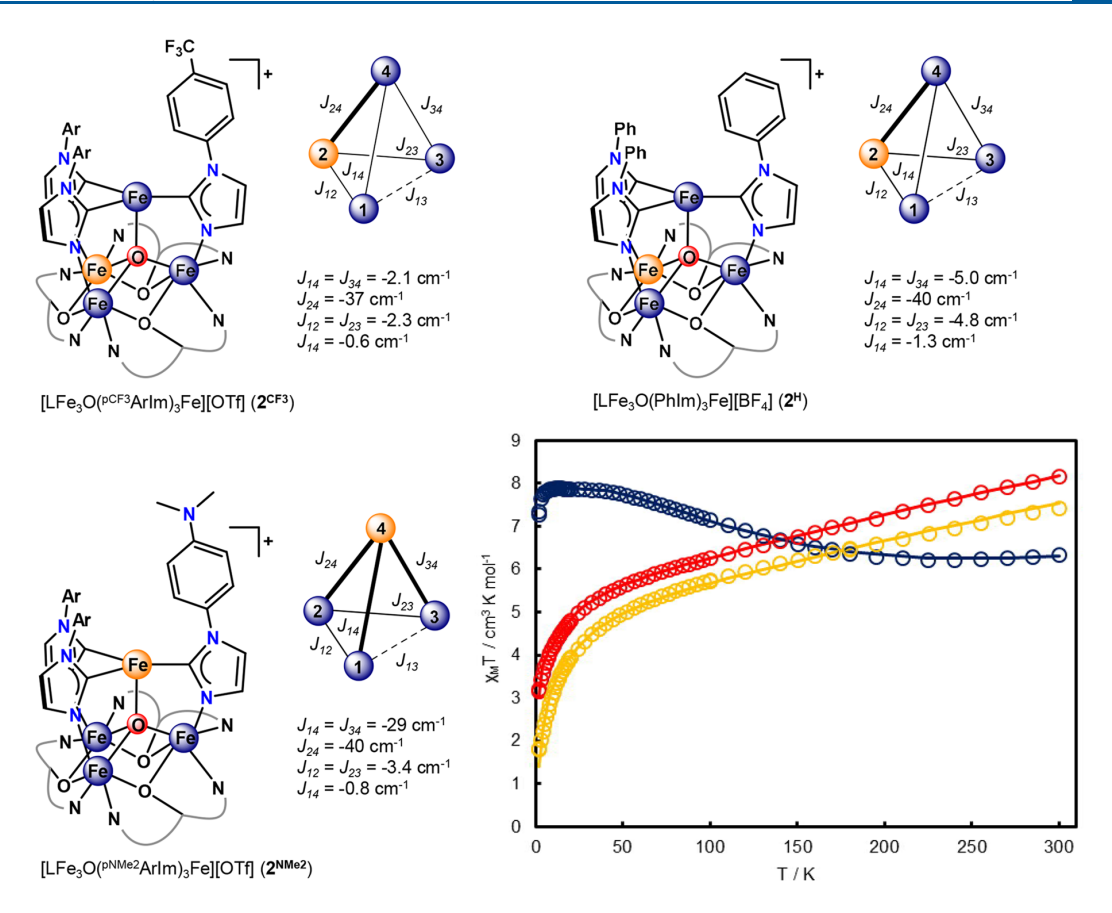


Figure 6. Redox distribution governs the magnetic properties in a series of site-differentiated $[LFe_3O(^RArIm)_3Fe]^+$ clusters. Exchange coupling model, fit parameters, and variable-temperature magnetic susceptibility data for 2^{CF3} (red trace), 2^H (orange trace), and 2^{NMe2} (blue trace). For additional simulation details, see the Supporting Information.

(Figure 6, orange trace) decrease monotonically with temperature, reaching values of 3.16 and 1.81 cm³ K mol⁻¹, respectively, at 1.8 K. No plateau is observed in the $\chi_{\rm M}T$ values down to 1.8-5 K, suggesting that neither 2^{CF3} nor 2^H possesses a well-isolated spin ground state. Simulations of the experimental data reveal significantly smaller $J_{14} = J_{34}$ coupling constants for 2^{CF3} and 2^{H} (-2.1 and -5 cm⁻¹, respectively) in comparison to 2^{NMe2} (-29 cm⁻¹). While the intracore exchange coupling remains weak $(J_{12} = J_{23} = -2.3 \text{ cm}^{-1}, J_{13} = -0.6 \text{ cm}^{-1} \text{ for } \mathbf{2}^{\text{CF3}}; J_{12} = J_{23} = -4.8 \text{ cm}^{-1}, J_{13} = -1.3 \text{ cm}^{-1} \text{ for } \mathbf{2}^{\text{H}})$, the smaller values of $J_{14} = J_{34}$ are no longer large enough to spin frustrate the triiron core. As a result, the calculated energy level diagrams for 2^{CF3} (Figure 57 in the Supporting Information) and 2^H (Figure 63 in the Supporting Information) indicate multiple low-lying excited states with energies as low as ca. 0.3 and 0.6 cm⁻¹, respectively (equivalent temperatures 0.4 and 0.9 K). This is in stark contrast to 2^{NMe2}, for which the first excited sextet state is predicted at ca. 120 cm⁻¹ (equivalent temperature 173 K, Figure 68 in the Supporting Information).

On the basis of the sensitivity of the spin ladder to $J_{14} = J_{34}$, the presence (or absence) of a well-isolated, high-spin ground state appears to be directly correlated with the oxidation state of the apical iron center. The dominant superexchange pathways within the $[LFe_3O(^RArIm)_3Fe]^+$ core are likely

through the monatomic bridging oxo ligand, and the strengths of these interactions are highly sensitive to the Fe-O bond lengths. 74-76 For 2CF3 and 2H, which feature apical FeII centers, the Fe4-O1 distance is elongated (0.04-0.06 Å) relative to 2^{NMe2} , which features an apical ferric site. The nearly identical values for J_{24} determined for 2^{CF3} (-37 cm⁻¹), 2^{H} (-40 cm⁻¹), and 2^{NMe2} (-40 cm⁻¹) suggest that changes in the Fe^{II}-Fe^{III} coupling constant due to elongation in the Fe4-O1 distance are largely compensated for by contraction of the Fe2-O1 bond length. However, elongation in the Fe4-O1 distance modulates the extent to which Fe4 is magnetically coupled with the ferrous centers of the triiron core (Fe1 and Fe3), thereby dictating whether or not the triiron core will be ferromagnetically aligned at low temperatures. Overall, our magnetostructural studies indicate that the spin ground state of site-differentiated iron clusters and its energetic isolation from excited states are indicators of electronic distribution, which we have shown can be systematically tuned by remote ligand modifications.

CO Reactivity: IR Spectroscopy. Crystallographic, spectroscopic, and magnetic studies indicate that localization of ferric character at the unique apical iron is preferred in the ground state of [LFe₃O(^RArIm)₃Fe]²⁺ clusters. Notwithstanding, we have previously shown that binding of CO induces an internal electron transfer from a distal Fe^{II} center, resulting in

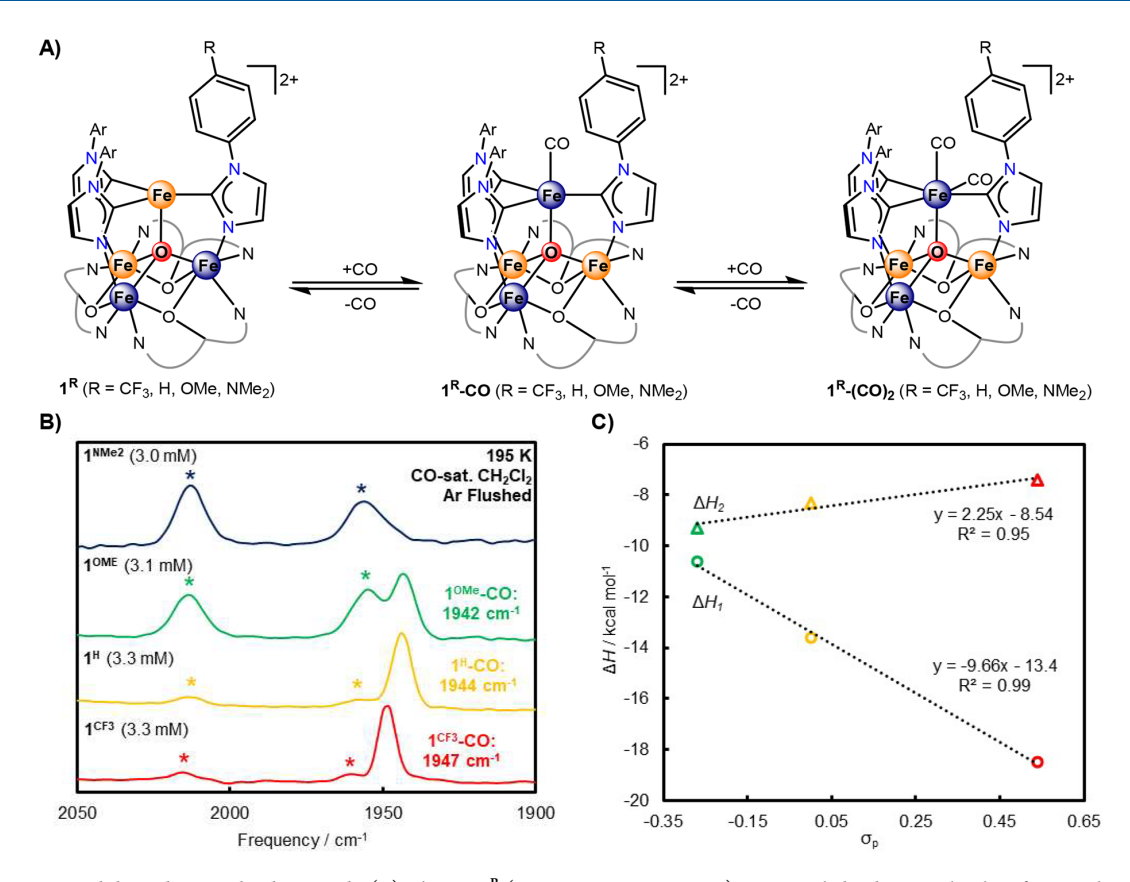


Figure 7. Ligand-dependent CO binding trends. (A) Clusters $\mathbf{1}^R$ (R = CF₃, H, OMe, NMe₂) successively bind two molecules of CO at the apical Fe4 site. For structural characterization of representative examples of mono- and dicarbonyl adducts, see ref 30. (B) Low-temperature IR spectroscopy illustrates the influence of ligand modifications on the affinity of $\mathbf{1}^R$ (R = CF₃, H, OMe, NMe₂) for binding one vs two molecules of CO. Asterisks denote features associated with the corresponding dicarbonyl species $\mathbf{1}^R$ -(CO)₂ (R = CF₃, H, OMe, NMe₂). For experimental details and variable-temperature data, see the Supporting Information. (C) Plot of the measured ΔH values for the first (bottom, circles) and second (top, triangles) CO binding events of $\mathbf{1}^{CF3}$ (red), $\mathbf{1}^H$ (orange), and $\mathbf{1}^{OMe}$ (green) vs the substituent Hammett σ_p parameters.

an apical Fe^{II}-CO motif as supported by Mössbauer and IR spectroscopy.³⁰ While internal electron transfer from a remote metal site accommodates coordination of CO at Fe^{III}, measurements of the CO binding energetics revealed that redox reorganization introduces a small energetic penalty to ligand binding. On the basis of the sensitivity of the redox distribution of 2^R (R = CF₃, H, OMe, NMe₂) to remote ligand modification, we reasoned that remote ligand modifications may also tune the propensity of [LFe₃O(^RArIm)₃Fe]²⁺ core to redistribute electron density, the extent of which may be determined by measuring the CO binding energetics of 1^R (R = CF₃, H, OMe, NMe₂). As such, we investigated the effect of remote ligand modifications on the reactivity of the Hammett series $\mathbf{1}^{R}$ (R = CF₃, H, OMe, NMe₂) with CO. The IR spectrum of 1^{CF3} at 195 K in CO-saturated dichloromethane (3.3 mM) following an Ar purge is qualitatively similar to that of 2^H (Figure 7B). An intense feature attributed to the formation of the monocarbonyl adduct 1^{CF3}-CO is observed at 1947 cm⁻¹ (in comparison to 1944 cm⁻¹ for 1^H-CO). Additionally, weak features at 1961 and 2015 cm⁻¹ indicate formation of the dicarbonyl complex 1^{CF3}-(CO)₂ (1960 and 2014 cm⁻¹ for 1^{H} -(CO)₂). When the solution is warmed to 273 K under Ar, the Fe-CO vibration of 1^{CF3} -CO at 1947 cm⁻¹ remains intense (Figure 23 in the Supporting Information). In analogous experiments with 1^{H} -CO, no diagnostic Fe–CO vibrations were discernible at 273 K, ³⁰ suggesting that the formation of the monocarbonyl complex is thermodynamically more favorable for 1^{CF3} in comparison to 1^{H} .

On the other hand, the IR spectrum of 1 OMe (Figure 7B) in CO-saturated dichloromethane under nearly identical conditions (3.1 mM, 195 K) exhibits three intense Fe-CO vibrational features. The lowest energy feature (1942 cm⁻¹) is attributable to the monocarbonyl complex 10Me-CO, with the remaining features at 1955 and 2013 cm⁻¹ assigned to the dicarbonyl adduct 1^{OMe} -(CO)₂. The higher relative intensity of these features indicates a larger binding constant for coordination of the second CO to 1 OMe in comparison to 1^{CF3} or 1^H. For the most electron rich cluster 1^{NMe²}, no welldefined features assignable to the monocarbonyl complex 1^{NMe2}-CO are observed, only those corresponding to the dicarbonyl adduct 1^{NMe2}-(CO)₂ at 1957 and 2013 cm⁻¹. The CO stretching frequencies of the mono- and dicarbonyl complexes are affected only slightly by the ligand changes $(1942-1947 \text{ cm}^{-1} \text{ for } \mathbf{1}^{R}\text{-CO}, R = CF_3, H, OMe; 1984-1988)$ cm⁻¹ as the average for $\mathbf{1}^{R}$ -(CO)₂, R = CF₃, H, OMe, NMe₂). The monocarbonyl species show increased activation of CO, as expected, with the more electron rich ligands. For dicarbonyl

Table 3. Thermodynamics of CO Binding to 1^R (R = CF₃, H, OMe, NMe₂) in Dichloromethane

| complex ^a | ligand | $K_{278\mathrm{K}} \; (\mathrm{atm}^{-1})^b$ | ΔH (kcal mol ⁻¹) | ΔS (cal mol ⁻¹ K ⁻¹) |
|-----------------------------------|--------|--|--------------------------------------|---|
| 1 ^{CF3c} | CO | 9.3 | -18.5(4) | -62(2) |
| $1^{\mathrm{H}d}$ | CO | 1.7 | -13.6(8) | -48(3) |
| $1^{\mathrm{OMe}e}$ | CO | 0.2 | -10.6(2) | -42(1) |
| $1^{\mathrm{NMe}2f}$ | 2 CO | 0.1 | -23.2(9) | -88(4) |
| 1^{CF3} - CO^g | CO | 0.1 | -7.4(1) | -31(1) |
| 1^{H} -CO c | CO | 0.2 | -8.3(5) | -32(2) |
| 1 ^{OMe} -CO ^f | CO | 0.5 | -9.3(3) | -35(1) |

^aStandard state: 1 atm of CO unless noted otherwise. ^bBinding energetics of 1^R (R = CF₃, H, OMe, NMe₂) were determined by ¹H NMR spectroscopy with [Fc*][OTf] as an internal standard in a sealed capillary tube. See the Supporting Information for more details. ^cBinding constants measured between 263 and 308 K. ^dData taken from ref 30. ^eBinding constants measured between 243 and 283 K. ^fBinding constants measured between 243 and 278 K. ^gBinding constants measured between 213 and 278 K.

species, the same trend holds for 1^R -(CO)₂ (R = CF₃, H, OMe, NMe₂). However, the opposing trends in the proportion of mono- and dicarbonyl species generated as a function of different ligands is unexpected. Despite the higher binding affinity of $1^{\rm OMe}$ and $1^{\rm NMe2}$ for two molecules of CO at 195 K, neither exhibit discernible Fe–CO vibrational features upon warming to 273 K (Figures 24 and 25 in the Supporting Information), suggesting a lower overall affinity for CO in comparison to $1^{\rm CF3}$ at this temperature.

CO Binding Energetics. The ligand-dependent trends in CO binding were confirmed by ¹H NMR spectroscopy. Cooling solutions of 1^{CF3} in dichloromethane-d₂ under an atmosphere of CO from 298 to 268 K predominately affords the monocarbonyl complex 1^{CF3}-CO as the major species (84% at 268 K, Figure 42 in the Supporting Information). Cooling beyond 268 K gradually converts 1^{CF3}-CO to the dicarbonyl complex 1^{CF3}-(CO)₂ (100% at 203 K). In comparison to 1^{CF3} , significantly lower conversion of 1^{OMe} to 10Me-CO is observed between 278 and 298 K (13% vs 82% at 278 K, Figure 42 in the Supporting Information) under an atmosphere of CO under identical conditions (8.8 mM in $CD_2C\overline{l}_2$, $P_{CO} = 1$ atm). Moreover, the presence of $\mathbf{1}^{OMe}$ (>5%) in solution down to 243 K indicates that 1^{OMe} has an overall affinity for CO lower than that of 1 CF3 in the temperature range 243-298 K. Whereas substantial amounts of 1^{CF3}-CO accumulate before significant quantities of 1^{CF3} -(CO)₂ are observed, the appearance of 1^{OMe} -CO and 1^{OMe} -(CO)₂ occurs almost simultaneously (19% vs 18%, respectively, at 268 K). As a result, full conversion of 1 OMe to the dicarbonyl complex 1^{OMe}-(CO)₂ is achieved at higher temperatures (223 K in comparison to 203 K for 1^{CF3}-(CO)₂). For the more electron rich 1^{NMe2}, ¹H NMR features associated with the corresponding monocarbonyl adduct 1^{NMe2}-CO are not observed at any temperature and full conversion to 1^{NMe2}-(CO)₂ occurs between 233 and 243 K (Figure 42 in the Supporting Information). This does not simply result from a large binding constant associated with the second coordination event (with K_1 being constant) because, like $\mathbf{1}^{OMe}$, the onset temperature for CO binding (ca. 268-278 K) is much lower than that for 1^{CF3} (>298 K). Thus, qualitatively, our variable-temperature ¹H NMR and IR studies indicate that the electronic effect of the remote ligand modifications have a disparate influence on the first and second CO binding events. Formation of the monocarbonyl adducts $[LFe_3O(^{R}ArIm)_3Fe(CO)]^{2+}$ is suppressed by electron-donating substituents, whereas formation of the dicarbonyl complexes [LFe₃O(^RArIm)₃Fe(CO)₂]²⁺ is enhanced.

To quantify the electronic effect of the remote ligand modifications, the CO binding energetics of 1^R (R = CF₃, H, OMe, NMe₂) were determined by ¹H NMR spectroscopy with [Fc*][OTf] as an internal standard in a sealed capillary tube. At 278 K, ⁷⁸ the CO binding constants of 1^R -(CO)₂ (R = CF₃, H, OMe) span nearly 2 orders of magnitude, decreasing monotonically from 9.3 atm⁻¹ for 1^{CF3} to 1.7 atm⁻¹ for 1^H and 0.2 atm⁻¹ for $\mathbf{1}^{\mathrm{OMe}}$ (all in dichloromethane- d_2 and $P_{\mathrm{CO}} = 1$ atm, Table 3). van't Hoff analysis reveals that formation of the monocarbonyl adducts 1^{R} -(CO) (R = CF₃, H, OMe) is associated with a large entropic penalty, which has previously been explained by the loss of rotational freedom in the flanking aryl substituents upon binding of CO.30 By comparison, the smaller entropic penalty associated with formation of the dicarbonyl adducts 1^R -(CO)₂ (R = CF₃, H, OMe) suggests that CO binding is cooperative, due to rotational "locking" of the aryl substituents following formation of the corresponding monocarbonyl adduct.

As is qualitatively suggested by our ¹H NMR and IR studies, the electronic character of the remote ligand substituents modulates the CO binding energetics of 1^R (R = CF₃, H, OMe), illustrated by the linear correlation of the measured ΔH values with the substituent Hammett σ_p parameters (Figure 7C). Notably, for a given substituent these effects are antithetical; electron-withdrawing substituents are associated with more negative ΔH values for the first CO binding event (formation of 1^R -CO, R = CF₃, H, OMe) but less negative ΔH values for the second CO binding event (formation of 1^R- $(CO)_2$, R = CF₃, H, OMe). Moreover, the first CO binding event ($\Delta \Delta H$ up to 7.9 kcal mol⁻¹) is ca. 4 times more sensitive to the electronic nature of the remote substituent than the second CO binding event ($\Delta\Delta H$ up to 1.9 kcal mol⁻¹). Although we are unable to directly measure the individual CO binding constants for 1 NMe2, we emphasize that its temperature-dependent CO binding profile is consistent with the trends observed for 1^R (R = CF₃, H, OMe). The onset temperature for CO binding to 1^{NMe2} is the lowest in the series, and complete conversion to the dicarbonyl $1^{\text{NMe}2}$ - $(CO)_2$ occurs at temperatures higher than those for 1^R (R = CF₃, H, OMe). This indicates that 1^{NMe2} has both the lowest K_1 and highest K_2 values, as anticipated on the basis of Figure 7C. For comparison, previous studies have shown that CO binding constants often increase as reduction potentials decrease, 79,80 which is attributed to the π -acidity of CO. Thus, the observation of the opposite trend in the formation constants for 1^R -CO (R = CF₃, H, OMe) is notable, especially since the donor strength of the bridging imidazolate was found to be crucial for enabling CO binding to 1^H in comparison to

structurally homologous clusters with less donating pyrazolate ligands. $^{30}\,$

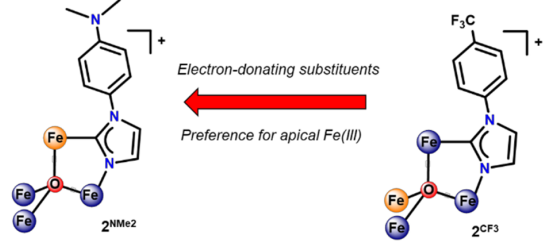
Insights into Ligand-Dependent CO Binding Trends. The linear correlation of the measured Fe-CO vibrational features with the Hammett substituent constants (Figure 26 in the Supporting Information) indicates that an electronic rearrangement occurs in 1^{CF3} and 1^{OMe} upon CO binding, analogous to that reported previously for 1^{H 30} We have proposed a thermodynamic model for ligand-induced redox reorganization which quantitatively describes the binding of CO at the apical Fe^{III} center of I^R (R = CF₃, H, OMe, NMe₂).³⁰ The measured ΔH values for the formation of $\mathbf{1}^{R}$ -CO ($R = CF_3$, H, OMe) can be decomposed into two terms, one arising from the energetic cost of redox reorganization and the other from the intrinsic affinity of the incipient localized Fe^{II} site for CO (Figure 8B). The sensitivity of the first CO binding event to the substituent σ_p parameter ($\Delta \Delta H = -4.9$ kcal mol⁻¹ for 1^{CF3} and +3.0 kcal mol⁻¹ for 1^{OMe}, relative to 1^H) indicates that the redox reorganization energy is significantly perturbed by remote ligand modifications.

Importantly, the second CO binding event of 1^R , R = CF_{3} , H, OMe (formation of 1^R -(CO)₂, R = CF₃, H, OMe, from 1^R - CO_1 , R = CF_3 , H, OMe) serves as an internal reference for the remote substituent effect on CO binding in the absence of redox reorganization. 81 The small $\Delta\Delta H$ values calculated for the second CO binding events of of 1^R (R = CF₃, H, OMe) (+0.9 kcal mol⁻¹ for 1^{CF3} and -1.0 kcal mol⁻¹ for 1^{OMe}, relative to 1^H) demonstrate that this intrinsic substituent influence is small, but the trend is consistent with the expectation that more reducing metal complexes should have a higher affinity for π -acids. ^{30,79,80} Assuming that the intrinsic substituent effects are similar for both the first and second CO binding events, the effect of remote ligand modification on the redox reorganization energy (RRE, relative to that for 1H) must be on the order of -5.8 kcal mol⁻¹ for 1^{CF3} and +4.0 kcal mol⁻¹ for 10Me. Thus, the incorporation of electron-donating substituents stabilizes ferric character at the apical metal site and increases the penalty associated with internal electronic rearrangements within the cluster which would formally reduce Fe4, resulting in an inverted linear free energy relationship for CO binding (Figure 8B(ii)).

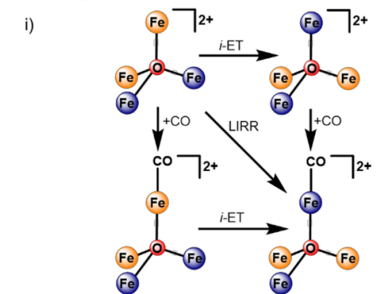
CONCLUSION

In summary, a series of site-differentiated iron clusters [LFe₃O(^RArIm)₃Fe][OTf]₂ with tunable electronic properties was synthesized, and binding of up to two molecules of CO was observed. The cluster's redox properties and CO stretching frequencies shift as expected on the basis of the electronic properties of the ligand: electron-donating substituents result in more reducing clusters and weaker C-O bonds. Moreover, the electronic character of a remote ligand substituent was found to significantly affect the energetics of CO binding ($\Delta\Delta H$ by as much as 7.9 kcal mol⁻¹) at a single ferric iron site within the cluster. Surprisingly, however, electron-donating substituents suppress the first CO binding event but enhance the second. Spectroscopic studies reveal that these substituent effects result from changes in the penalty associated with electronic redistribution, which is an essential feature of the first CO binding event. To the best of our knowledge, the clusters discussed herein are the first to simultaneously exhibit "normal" and inverted free energy relationships for CO binding. This unique feature of multimetallic complexes which must undergo electronic

A) Remote Ligand Modifications Govern Electronic Distribution



B) Remote Ligand Modifications Tune Electronic Redistribution



 $\Delta \Delta H_{LIRR} = \Delta \Delta H_{RRE} + \Delta \Delta H_{CO}$

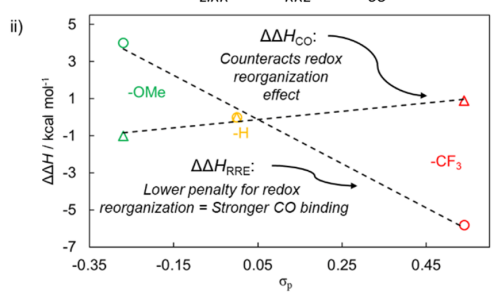


Figure 8. (A) Summary of the effect of remote ligand modifications on the electronic distribution of $\mathbf{1}^R$ (R = CF₃, H, OMe, NMe₂). (B) (i) Thermodynamic model for binding of CO to $\mathbf{1}^R$ (R = CF₃, H, OMe, NMe₂), coupled to an internal redox reorganization, which can be used to estimate the effect of remote ligand substitution of the redox reorganization energies of $\mathbf{1}^R$ (R = CF₃, H, OMe, NMe₂). (ii) Plot of the $\Delta\Delta H_{RRE}$ (circles) and $\Delta\Delta H_{CO}$ (triangles) values for $\mathbf{1}^{CF3}$ (red), $\mathbf{1}^H$ (orange), and $\mathbf{1}^{OMe}$ (green) vs the substituent Hammett σ_p parameters ($\mathbf{1}^H$ is set to 0 for reference). Abbreviations: i-ET = internal electron transfer/redox reorganization, LIRR = ligand-induced redox reorganization, RRE = redox reorganization energy.

rearrangement to accommodate small-molecule binding could be potentially useful in controlling product selectivity, for example in the reduction of CO to hydrocarbons, by providing a means to independently tune sequential CO binding constants. Because More broadly, the unusual ligand-dependent trends in diatomic binding reported herein highlight how the first and/or second coordination sphere of a transition-metal cluster could be rationally tuned to flip traditional thermodynamic scaling relationships toward controlling small-molecule activation.

ASSOCIATED CONTENT

Supporting Information

The Supporting Information is available free of charge on the ACS Publications website at DOI: 10.1021/acs.inorg-chem.9b02470.

Synthetic procedures, characterization data and crystal structures, spectroscopic and electrochemical results, and CO reactivity studies (PDF)

Accession Codes

CCDC 1934987–1934990 contain the supplementary crystallographic data for this paper. These data can be obtained free of charge via www.ccdc.cam.ac.uk/data_request/cif, or by emailing data_request@ccdc.cam.ac.uk, or by contacting The Cambridge Crystallographic Data Centre, 12 Union Road, Cambridge CB2 1EZ, UK; fax: +44 1223 336033.

AUTHOR INFORMATION

Corresponding Author

*E-mail for T.A.: agapie@caltech.edu.

ORCID (

Theodor Agapie: 0000-0002-9692-7614

Notes

The authors declare no competing financial interest.

ACKNOWLEDGMENTS

This research was supported by the NSF (CHE-1905320). T.A. is grateful for a Dreyfus fellowship. C.H.A. is grateful for an NSF Graduate Research Fellowship. We acknowledge the Gordon and Betty Moore Foundation and the Beckman Institute for their generous support of the Molecular Observatory at Caltech. Diffraction data was collected at the X-ray Crystallography Facility in the Beckman Institute at Caltech, which is supported by a Dow Next Generation Instrument Grant. Operations at SSRL are supported by the US DOE and NIH. We thank Michael Takase and Lawrence Henling for assistance with crystallography, Paul Oyala for assistance with EPR spectroscopy, and Matthew Chalkley and Dirk Schild for assistance with Mössbauer spectroscopy.

■ REFERENCES

- (1) Cook, S. A.; Borovik, A. S. Molecular Designs for Controlling the Local Environments around Metal Ions. *Acc. Chem. Res.* **2015**, 48 (8), 2407–2414.
- (2) Mirts, E. N.; Bhagi-Damodaran, A.; Lu, Y. Understanding and Modulating Metalloenzymes with Unnatural Amino Acids, Non-Native Metal Ions, and Non-Native Metallocofactors. *Acc. Chem. Res.* **2019**, 52 (4), 935–944.
- (3) Barlow, J. M.; Yang, J. Y. Thermodynamic Considerations for Optimizing Selective CO2 Reduction by Molecular Catalysts. ACS Cent. Sci. 2019, 5 (4), 580–588.
- (4) Warren, J. J.; Tronic, T. A.; Mayer, J. M. Thermochemistry of Proton-Coupled Electron Transfer Reagents and its Implications. *Chem. Rev.* **2010**, *110* (12), 6961–7001.
- (5) Ostericher, A. L.; Waldie, K. M.; Kubiak, C. P. Utilization of Thermodynamic Scaling Relationships in Hydricity To Develop Nickel Hydrogen Evolution Reaction Electrocatalysts with Weak Acids and Low Overpotentials. ACS Catal. 2018, 8 (10), 9596–9603.
- (6) Azcarate, I.; Costentin, C.; Robert, M.; Savéant, J.-M. Dissection of Electronic Substituent Effects in Multielectron-Multistep Molecular Catalysis. Electrochemical CO2-to-CO Conversion Catalyzed by Iron Porphyrins. *J. Phys. Chem. C* **2016**, 120 (51), 28951–28960.
- (7) Pegis, M. L.; McKeown, B. A.; Kumar, N.; Lang, K.; Wasylenko, D. J.; Zhang, X. P.; Raugei, S.; Mayer, J. M. Homogenous Electrocatalytic Oxygen Reduction Rates Correlate with Reaction Overpotential in Acidic Organic Solutions. ACS Cent. Sci. 2016, 2 (11), 850–856.
- (8) Passard, G.; Ullman, A. M.; Brodsky, C. N.; Nocera, D. G. Oxygen Reduction Catalysis at a Dicobalt Center: The Relationship

- of Faradaic Efficiency to Overpotential. J. Am. Chem. Soc. 2016, 138 (9), 2925–2928.
- (9) Chantarojsiri, T.; Ziller, J. W.; Yang, J. Y. Incorporation of redoxinactive cations promotes iron catalyzed aerobic C-H oxidation at mild potentials. *Chem. Sci.* **2018**, 9 (9), 2567–2574.
- (10) Chantarojsiri, T.; Reath, A. H.; Yang, J. Y. Cationic Charges Leading to an Inverse Free-Energy Relationship for N-N Bond Formation by MnVI Nitrides. *Angew. Chem., Int. Ed.* **2018**, 57 (43), 14037–14042.
- (11) Azcarate, I.; Costentin, C.; Robert, M.; Savéant, J.-M. Through-Space Charge Interaction Substituent Effects in Molecular Catalysis Leading to the Design of the Most Efficient Catalyst of CO2-to-CO Electrochemical Conversion. *J. Am. Chem. Soc.* **2016**, *138* (51), 16639–16644.
- (12) Pegis, M. L.; Wise, C. F.; Koronkiewicz, B.; Mayer, J. M. Identifying and Breaking Scaling Relations in Molecular Catalysis of Electrochemical Reactions. *J. Am. Chem. Soc.* **2017**, *139* (32), 11000–11003
- (13) Waidmann, C. R.; Miller, A. J. M.; Ng, C.-W. A.; Scheuermann, M. L.; Porter, T. R.; Tronic, T. A.; Mayer, J. M. Using combinations of oxidants and bases as PCET reactants: thermochemical and practical considerations. *Energy Environ. Sci.* **2012**, *5* (7), 7771–7780.
- (14) Rebelein, J. G.; Lee, C. C.; Newcomb, M.; Hu, Y.; Ribbe, M. W. Characterization of an M-Cluster-Substituted Nitrogenase VFe Protein. *mBio* 2018, 9 (2), No. e00310-18.
- (15) Spatzal, T.; Schlesier, J.; Burger, E.-M.; Sippel, D.; Zhang, L.; Andrade, S. L. A.; Rees, D. C.; Einsle, O. Nitrogenase FeMoco investigated by spatially resolved anomalous dispersion refinement. *Nat. Commun.* **2016**, *7*, 10902.
- (16) Spatzal, T.; Einsle, O.; Andrade, S. L. A. Analysis of the Magnetic Properties of Nitrogenase FeMo Cofactor by Single-Crystal EPR Spectroscopy. *Angew. Chem., Int. Ed.* **2013**, *52* (38), 10116–10119.
- (17) Hoffman, B. M.; Lukoyanov, D.; Yang, Z.-Y.; Dean, D. R.; Seefeldt, L. C. Mechanism of Nitrogen Fixation by Nitrogenase: The Next Stage. *Chem. Rev.* **2014**, *114* (8), 4041–4062.
- (18) McEvoy, J. P.; Brudvig, G. W. Water-Splitting Chemistry of Photosystem II. Chem. Rev. 2006, 106 (11), 4455–4483.
- (19) Lubitz, W.; Ogata, H.; Rüdiger, O.; Reijerse, E. Hydrogenases. Chem. Rev. 2014, 114 (8), 4081–4148.
- (20) Ragsdale, S. W. Metals and Their Scaffolds To Promote Difficult Enzymatic Reactions. Chem. Rev. 2006, 106 (8), 3317–3337.
- (21) Hakulinen, N.; Kiiskinen, L.-L.; Kruus, K.; Saloheimo, M.; Paananen, A.; Koivula, A.; Rouvinen, J. Crystal structure of a laccase from Melanocarpus albomyces with an intact trinuclear copper site. *Nat. Struct. Biol.* **2002**, *9* (8), 601–605.
- (22) Ferguson-Miller, S.; Babcock, G. T. Heme/Copper Terminal Oxidases. Chem. Rev. 1996, 96 (7), 2889–2908.
- (23) Cammarota, R. C.; Xie, J.; Burgess, S. A.; Vollmer, M. V.; Vogiatzis, K. D.; Ye, J.; Linehan, J. C.; Appel, A. M.; Hoffmann, C.; Wang, X.; Young, V. G.; Lu, C. C. Thermodynamic and kinetic studies of H2 and N2 binding to bimetallic nickel-group 13 complexes and neutron structure of a Ni(η 2-H2) adduct. *Chem. Sci.* **2019**, *10*, 7029.
- (24) Cammarota, R. C.; Clouston, L. J.; Lu, C. C. Leveraging molecular metal-support interactions for H2 and N2 activation. *Coord. Chem. Rev.* **2017**, 334, 100–111.
- (25) Zhang, H.; Hatzis, G. P.; Moore, C. E.; Dickie, D. A.; Bezpalko, M. W.; Foxman, B. M.; Thomas, C. M. O2 Activation by a Heterobimetallic Zr/Co Complex. J. Am. Chem. Soc. 2019, 141, 9516.
- (26) Krogman, J. P.; Bezpalko, M. W.; Foxman, B. M.; Thomas, C. M. Multi-electron redox processes at a Zr(iv) center facilitated by an appended redox-active cobalt-containing metalloligand. *Dalton Trans* **2016**, *4*5 (27), 11182–11190.
- (27) Xue, G.; De Hont, R.; Münck, E.; Que, L., Jr Million-fold activation of the $[Fe_2(\mu-O)_2]$ diamond core for C-H bond cleavage. *Nat. Chem.* **2010**, *2*, 400.

(28) Camara, J. M.; Rauchfuss, T. B. Combining acid-base, redox and substrate binding functionalities to give a complete model for the [FeFe]-hydrogenase. *Nat. Chem.* **2012**, *4*, 26.

- (29) Cammarota, R. C.; Lu, C. C. Tuning Nickel with Lewis Acidic Group 13 Metalloligands for Catalytic Olefin Hydrogenation. *J. Am. Chem. Soc.* **2015**, 137 (39), 12486–12489.
- (30) Arnett, C. H.; Chalkley, M. J.; Agapie, T. A Thermodynamic Model for Redox-Dependent Binding of Carbon Monoxide at Site-Differentiated, High Spin Iron Clusters. *J. Am. Chem. Soc.* **2018**, *140* (16), 5569–5578.
- (31) Reed, C. J.; Agapie, T. Tetranuclear Fe Clusters with a Varied Interstitial Ligand: Effects on the Structure, Redox Properties, and Nitric Oxide Activation. *Inorg. Chem.* **2017**, *56* (21), 13360–13367.
- (32) de Ruiter, G.; Thompson, N. B.; Lionetti, D.; Agapie, T. Nitric Oxide Activation by Distal Redox Modulation in Tetranuclear Iron Nitrosyl Complexes. *J. Am. Chem. Soc.* **2015**, *137* (44), 14094–14106.
- (33) Reed, C. J.; Agapie, T. A Terminal FeIII-Oxo in a Tetranuclear Cluster: Effects of Distal Metal Centers on Structure and Reactivity. *J. Am. Chem. Soc.* **2019**, *141*, 9479.
- (34) Reed, C. J.; Agapie, T. Thermodynamics of Proton and Electron Transfer in Tetranuclear Clusters with Mn-OH₂/OH Motifs Relevant to H₂O Activation by the Oxygen Evolving Complex in Photosystem II. J. Am. Chem. Soc. **2018**, 140 (34), 10900–10908.
- (35) de Ruiter, G.; Carsch, K. M.; Gul, S.; Chatterjee, R.; Thompson, N. B.; Takase, M. K.; Yano, J.; Agapie, T. Accelerated Oxygen Atom Transfer and C-H Bond Oxygenation by Remote Redox Changes in Fe₃Mn-Iodosobenzene Adducts. *Angew. Chem., Int. Ed.* **2017**, *56* (17), 4772–4776.
- (36) Holm, R. H.; Lo, W. Structural Conversions of Synthetic and Protein-Bound Iron-Sulfur Clusters. *Chem. Rev.* **2016**, *116* (22), 13685–13713.
- (37) Hernández Sánchez, R.; Zheng, S.-L.; Betley, T. A. Ligand Field Strength Mediates Electron Delocalization in Octahedral $[(^{H}L)_{2}Fe_{6}(L')_{m}]^{n+}$ Clusters. *J. Am. Chem. Soc.* **2015**, *137* (34), 11126–11143.
- (38) Eames, E. V.; Harris, T. D.; Betley, T. A. Modulation of magnetic behavior via ligand-field effects in the trigonal clusters (PhL)Fe3L*3 (L* = thf, py, PMe2Ph). *Chem. Sci.* **2012**, 3 (2), 407–415.
- (39) Anderton, K. J.; Ermert, D. M.; Quintero, P. A.; Turvey, M. W.; Fataftah, M. S.; Abboud, K. A.; Meisel, M. W.; Čižmár, E.; Murray, L. J. Correlating Bridging Ligand with Properties of Ligand-Templated $[Mn^{II}_3X_3]^{3+}$ Clusters (X = Br-, Cl-, H-, MeO-). *Inorg. Chem.* **2017**, 56 (19), 12012–12022.
- (40) Lee, H. B.; Agapie, T. Redox Tuning via Ligand-Induced Geometric Distortions at a YMn₃O₄Cubane Model of the Biological Oxygen Evolving Complex. *Inorg. Chem.* **2019**, DOI: 10.1021/acs.inorgchem.9b00510.
- (41) Lee, H. B.; Shiau, A. A.; Oyala, P. H.; Marchiori, D. A.; Gul, S.; Chatterjee, R.; Yano, J.; Britt, R. D.; Agapie, T. Tetranuclear [Mn^{III}Mn₃^{IV}O₄] Complexes as Spectroscopic Models of the S2 State of the Oxygen Evolving Complex in Photosystem II. *J. Am. Chem. Soc.* **2018**, *140* (49), 17175–17187.
- (42) Stack, T. D. P.; Holm, R. H. Subsite-differentiated analogs of biological [4Fe-4S]²⁺ clusters: synthesis, solution and solid-state structures, and subsite-specific reactions. *J. Am. Chem. Soc.* **1988**, *110* (8), 2484–2494.
- (43) Stack, T. D. P.; Holm, R. H. Subsite-specific functionalization of the [4Fe-4S]²⁺ analog of iron-sulfur protein clusters. *J. Am. Chem. Soc.* **1987**, 109 (8), 2546–2547.
- (44) Zhao, Q.; Harris, T. D.; Betley, T. A. $[(HL)_2Fe_6(NCMe)_m]^{n+}$ (m = 0, 2, 4, 6; n = -1, 0, 1, 2, 3, 4, 6): An Electron-Transfer Series Featuring Octahedral Fe6 Clusters Supported by a Hexaamide Ligand Platform. *J. Am. Chem. Soc.* **2011**, 133 (21), 8293–8306.
- (45) Zhao, Q.; Betley, T. A. Synthesis and Redox Properties of Triiron Complexes Featuring Strong Fe-Fe Interactions. *Angew. Chem., Int. Ed.* **2011**, *50* (3), 709–712.
- (46) Guillet, G. L.; Sloane, F. T.; Ermert, D. M.; Calkins, M. W.; Peprah, M. K.; Knowles, E. S.; Čižmár, E.; Abboud, K. A.; Meisel, M.

- W.; Murray, L. J. Preorganized assembly of three iron(ii) or manganese(ii) β -diketiminate complexes using a cyclophane ligand. *Chem. Commun.* **2013**, 49 (59), 6635–6637.
- (47) McSkimming, A.; Suess, D. L. M. Selective Synthesis of Site-Differentiated Fe_4S_4 and Fe_6S_6 Clusters. *Inorg. Chem.* **2018**, *57* (23), 14904–14912.
- (48) Hansch, C.; Leo, A.; Taft, R. W. A survey of Hammett substituent constants and resonance and field parameters. *Chem. Rev.* **1991**, *91* (2), 165–195.
- (49) We have elected to conduct thorough spectroscopic studies at the extremes of the Hammett series in order to elucidate the effects of the ligand substituents on the electronic structure of the clusters.
- (50) Full spectroscopic characterization was performed on the extremes of the Hammett series.
- (51) de Ruiter, G.; Thompson, N. B.; Takase, M. K.; Agapie, T. Intramolecular C-H and C-F Bond Oxygenation Mediated by a Putative Terminal Oxo Species in Tetranuclear Iron Complexes. *J. Am. Chem. Soc.* **2016**, *138* (5), 1486–1489.
- (52) Venkateswara Rao, P.; Holm, R. H. Synthetic Analogues of the Active Sites of Iron-Sulfur Proteins. *Chem. Rev.* **2004**, *104* (2), 527–560
- (53) Chakrabarti, M.; Deng, L.; Holm, R. H.; Münck, E.; Bominaar, E. L. Mössbauer, Electron Paramagnetic Resonance, and Theoretical Studies of a Carbene-Based All-Ferrous Fe4S4 Cluster: Electronic Origin and Structural Identification of the Unique Spectroscopic Site. *Inorg. Chem.* **2009**, 48 (7), 2735–2747.
- (54) Yoo, S. J.; Angove, H. C.; Burgess, B. K.; Hendrich, M. P.; Münck, E. Mössbauer and Integer-Spin EPR Studies and Spin-Coupling Analysis of the [4Fe-4S]⁰ Cluster of the Fe Protein from Azotobacter vinelandii Nitrogenase. *J. Am. Chem. Soc.* **1999**, *121* (11), 2534–2545.
- (55) Angove, H. C.; Yoo, S. J.; Burgess, B. K.; Münck, E. Mössbauer and EPR Evidence for an All-Ferrous Fe4S4 Cluster with S = 4 in the Fe Protein of Nitrogenase. *J. Am. Chem. Soc.* **1997**, *119* (37), 8730–8731.
- (56) Münck, E.; Ksurerus, K.; Hendrich, M. P. Combining Mössbauer spectroscopy with integer spin electron paramagnetic resonance. *Methods Enzymol.* **1993**, 227, 463–479.
- (57) Surerus, K. K.; Hendrich, M. P.; Christie, P. D.; Rottgardt, D.; Orme-Johnson, W. H.; Munck, E. Moessbauer and integer-spin EPR of the oxidized P-clusters of nitrogenase: POX is a non-Kramers system with a nearly degenerate ground doublet. *J. Am. Chem. Soc.* 1992, 114 (22), 8579–8590.
- (58) Hendrich, M. P.; Debrunner, P. G. Integer-spin electron paramagnetic resonance of iron proteins. *Biophys. J.* **1989**, *56* (3), 489–506.
- (59) Sutradhar, M.; Carrella, L. M.; Rentschler, E. A Discrete μ_4 -Oxido Tetranuclear Iron(III) Cluster. *Eur. J. Inorg. Chem.* **2012**, 2012 (27), 4273–4278.
- (60) Murali, M.; Nayak, S.; Costa, J. S.; Ribas, J.; Mutikainen, I.; Turpeinen, U.; Clémancey, M.; Garcia-Serres, R.; Latour, J.-M.; Gamez, P.; Blondin, G.; Reedijk, J. Discrete Tetrairon(III) Cluster Exhibiting a Square-Planar Fe₄(μ_4 -O) Core: Structural and Magnetic Properties. *Inorg. Chem.* **2010**, *49* (5), 2427–2434.
- (61) Singh, A. K.; Jacob, W.; Boudalis, A. K.; Tuchagues, J.-P.; Mukherjee, R. A Tetragonal Core with Asymmetric Iron Environments Supported Solely by Bis(μ-OH){μ-(O-H···O)} Bridging and Terminal Pyridine Amide (N, O) Coordination: A New Member of the Tetrairon(III) Family. Eur. J. Inorg. Chem. 2008, 2008 (18), 2820–2829.
- (62) Chardon-Noblat, S.; Horner, O.; Chabut, B.; Avenier, F.; Debaecker, N.; Jones, P.; Pécaut, J.; Dubois, L.; Jeandey, C.; Oddou, J.-L.; Deronzier, A.; Latour, J.-M. Spectroscopic and Electrochemical Characterization of an Aqua Ligand Exchange and Oxidatively Induced Deprotonation in Diiron Complexes. *Inorg. Chem.* **2004**, 43 (5), 1638–1648.
- (63) Borovik, A. S.; Murch, B. P.; Que, L.; Papaefthymiou, V.; Munck, E. Models for iron-oxo proteins: a mixed valence iron(II)-iron(III) complex. J. Am. Chem. Soc. 1987, 109 (23), 7190-7191.

(64) Gütlich, P.; Bill, E.; Trautwein, A. X. Mössbauer Spectroscopy and Transition Metal Chemistry: Fundamentals and Applications; Springer: Berlin, 2011.

- (65) Smith, J. M.; Mayberry, D. E.; Margarit, C. G.; Sutter, J.; Wang, H.; Meyer, K.; Bontchev, R. P. N-O Bond Homolysis of an Iron(II) TEMPO Complex Yields an Iron(III) Oxo Intermediate. *J. Am. Chem. Soc.* 2012, 134 (15), 6516–6519.
- (66) Vogel, C.; Heinemann, F. W.; Sutter, J.; Anthon, C.; Meyer, K. An Iron Nitride Complex. *Angew. Chem., Int. Ed.* **2008**, 47 (14), 2681–2684.
- (67) Einsle, O.; Andrade, S. L. A.; Dobbek, H.; Meyer, J.; Rees, D. C. Assignment of Individual Metal Redox States in a Metalloprotein by Crystallographic Refinement at Multiple X-ray Wavelengths. *J. Am. Chem. Soc.* **2007**, *129* (8), 2210–2211.
- (68) Hendrickson, W. Determination of macromolecular structures from anomalous diffraction of synchrotron radiation. *Science* **1991**, 254 (5028), 51–58.
- (69) Wenke, B. B.; Spatzal, T.; Rees, D. C. Site-Specific Oxidation State Assignments of the Iron Atoms in the [4Fe:4S]^{2+/1+/0} States of the Nitrogenase Fe-Protein. *Angew. Chem., Int. Ed.* **2019**, 58 (12), 3894–3897.
- (70) Hernández Sánchez, R.; Champsaur, A. M.; Choi, B.; Wang, S. G.; Bu, W.; Roy, X.; Chen, Y.-S.; Steigerwald, M. L.; Nuckolls, C.; Paley, D. W. Electron Cartography in Clusters. *Angew. Chem., Int. Ed.* **2018**, *57* (42), 13815–13820.
- (71) Wu, G.; Zhang, Y.; Ribaud, L.; Coppens, P.; Wilson, C.; Iversen, B. B.; Larsen, F. K. Multitemperature Resonance-Diffraction and Structural Study of the Mixed-Valence Complex [Fe₃O(OOCC-(CH₃)₃)₆(C₅H₅N)₃]. *Inorg. Chem.* **1998**, *37* (23), 6078–6083.
- (72) Gao, Y.; Frost-Jensen, A.; Pressprich, M. R.; Coppens, P.; Marquez, A.; Dupuis, M. Valence contrast by synchrotron resonance scattering: application to a mixed-valence manganese compound. *J. Am. Chem. Soc.* **1992**, 114 (23), 9214–9215.
- (73) Bartholomew, A. K.; Teesdale, J. J.; Hernández Sánchez, R.; Malbrecht, B. J.; Juda, C. E.; Ménard, G.; Bu, W.; Iovan, D. A.; Mikhailine, A. A.; Zheng, S.-L.; Sarangi, R.; Wang, S. G.; Chen, Y.-S.; Betley, T. A. Exposing the inadequacy of redox formalisms by resolving redox inequivalence within isovalent clusters. *Proc. Natl. Acad. Sci. U. S. A.* **2019**, *116* (32), 15836–15841.
- (74) Mitchell, K. J.; Abboud, K. A.; Christou, G. Magnetostructural Correlation for High-Nuclearity Iron(III)/Oxo Complexes and Application to Fe5, Fe6, and Fe8 Clusters. *Inorg. Chem.* **2016**, *55* (13), 6597–6608.
- (75) Weihe, H.; Güdel, H. U. Angular and Distance Dependence of the Magnetic Properties of Oxo-Bridged Iron(III) Dimers. J. Am. Chem. Soc. 1997, 119 (28), 6539–6543.
- (76) Gorun, S. M.; Lippard, S. J. Magnetostructural correlations in magnetically coupled (μ -oxo)diiron(III) complexes. *Inorg. Chem.* **1991**, 30 (7), 1625–1630.
- (77) We have previously reported structural characterization of the analogous dicarbonyl complex 1^H-(CO)₂ and demonstrated that both CO molecules bind Fe4. The ¹H NMR features of the monocarbonyl complex 1^H-CO are nearly identical with those of the isoelectronic, structurally homologous pyrazolate-bridged nitrosyl compound [LFe₃O(PhPz)₃Fe][OTf₂], which has been structurally characterized. Moreover, the 1e⁻ reduced monocarbonyl 2^H-CO has been structurally characterized, revealing that CO binds trans to O1 as expected. Thus, variable-temperature ¹H NMR and IR spectroscopy in combination with XRD studies has defined the spectroscopic signatures expected for the carbonyl adducts discussed herein.
- (78) This temperature was selected for comparison because it is the highest temperature for which the first and second CO binding constants of 1^R (where relevant) may be measured directly.
- (79) Fujita, E.; Creutz, C.; Sutin, N.; Szalda, D. J. Carbon dioxide activation by cobalt(I) macrocycles: factors affecting carbon dioxide and carbon monoxide binding. *J. Am. Chem. Soc.* **1991**, *113* (1), 343–353.
- (80) Guo, R.-H.; Liu, C.-F.; Wei, T.-C.; Hu, C.-C. Electrochemical behavior of CO2 reduction on palladium nanoparticles: Dependence

- of adsorbed CO on electrode potential. *Electrochem. Commun.* **2017**, 80, 24–28.
- (81) The Mossbauer spectrum of 1^H-(CO)₂ is consistent with an Fe(II) formulation for the apical iron center, indicating that the overall redox distribution in the dicarbonyl complexes is the same as that in the monocarbonyl complexes. See ref 30.
- (82) Lee, C. C.; Wilcoxen, J.; Hiller, C. J.; Britt, R. D.; Hu, Y. Evaluation of the Catalytic Relevance of the CO-Bound States of V-Nitrogenase. *Angew. Chem., Int. Ed.* **2018**, *57* (13), 3411–3414.